Hyperon couplings from $N_f = 2+1$ lattice QCD

Gunnar S. Bali[a]**, Sara Collins**[a]**, Piotr Korcyl**[ab]**, Rudolf Rödl**[a]**, Simon Weishäupl**[*a] **and Thomas Wurm**[a]

[a]*Institut für Theoretische Physik, Universität Regensburg, 93040 Regensburg, Germany*
[b]*Marian Smoluchowski Institute of Physics, Jagiellonian University, ul. Łojasiewicza 11,*
30-348 Kraków, Poland
E-mail: gunnar.bali@ur.de, sara.collins@ur.de,
piotr.korcyl@uj.edu.pl, rudolf.roedl@ur.de, simon.weishaeupl@ur.de,
thomas.wurm@ur.de

We compute various (generalized) isovector charges of the octet baryons. These include g_A, g_T and g_S as well as the unpolarized, polarized and transversity parton distribution function (PDF) momentum fractions $\langle x \rangle_{u^+ - d^+}$, $\langle x \rangle_{\Delta u^- - \Delta d^-}$ and $\langle x \rangle_{\delta u^+ - \delta d^+}$. The simulations are carried out on a subset of the (isospin symmetric) $N_f = 2+1$ flavour Coordinated Lattice Simulations (CLS) gauge ensembles with lattice spacings ranging from $a \approx 0.086\,\text{fm}$ down to $a \approx 0.050\,\text{fm}$. First results on the breaking of flavour symmetry and the low energy constants F and D are presented. While SU(3) flavour symmetry violations are found to be sizeable for $g_A = \langle \mathbb{1} \rangle_{\Delta u^+ - \Delta d^+}$, these are quite small for $g_T = \langle \mathbb{1} \rangle_{\delta u^- - \delta d^-}$ and $\langle x \rangle_{u^+ - d^+}$.

---

*Speaker.

1. Introduction

In recent years quite a few lattice calculations of the nucleon axial charge g_A^N have been carried out, assuming isospin symmetry, most of which are compatible with the experimental ratio $g_A^N/g_V^N = 1.2732(23)$ [1], as measured from neutron β decay. On the lattice g_A^N can be accessed, e.g., via the proton matrix element $\langle p|\bar{u}\gamma_5\gamma_\mu u - \bar{d}\gamma_5\gamma_\mu d|p\rangle$. The hyperon axial charges g_A^B for $B \neq N$ are less well known since a direct measurement, e.g., of $\Sigma^- \to \Sigma^0 e^- \bar{\nu}_e$, is unrealistic. So far these can only be inferred, assuming an approximate flavour symmetry, from β decays such as $\Xi^- \to \Lambda \ell \bar{\nu}_\ell$ or $\Sigma^- \to n\ell\bar{\nu}_\ell$, where an s-quark is converted into a u-quark. In terms of lattice simulations only few direct results [2, 3, 4, 5, 6, 7] of these charges exist. Such determinations, however, are interesting both in terms of testing the extent of SU(3) flavour symmetry and to determine the low energy constants (LECs) F and D from first principles, which also appear in other SU(3) BChPT expansions, e.g., of octet baryon self-energies.

In addition to the axial charges we also compute the hyperon isovector charges in other channels, in particular the scalar charges g_S^B, and the tensor charges g_T^B as well as the unpolarized, polarized and transversity Bjorken momentum fractions $\langle x \rangle_{u^+-d^+}^B$, $\langle x \rangle_{\Delta u^- - \Delta d^-}^B$ and $\langle x \rangle_{\delta u^+ - \delta d^+}^B$, respectively, where $q^\pm = q \pm \bar{q}$. Much less is known for these (generalized) charges since these are even more elusive to experimental measurement than g_A^B.

2. CLS gauge ensembles used

Ensemble	β	a[fm]	$N_t \cdot N_s^3$	M_π[MeV]	LM_π	t/a	N_{configs}
● H102	3.4	0.0856	$96 \cdot 32^3$	355	4.9	[8(2), 10(2), 12(2), 14(2)]	2004
▲ N202	3.55	0.0642	$128 \cdot 48^3$	412	6.4	[11, 14(2), 16(2), 19(4)]	1768
▲ X250			$64 \cdot 48^3$	348	5.4	[11, 14(2), 16(4), 19(4)]	345
▲ X251			$64 \cdot 48^3$	269	4.2	[11, 14(2), 16(4), 19(4)]	436
● N203			$128 \cdot 48^3$	346	5.4	[11(2), 14(2), 16(2), 19(2)]	1543
● N200			$128 \cdot 48^3$	284	4.4	[11, 14, 16, 19]	1712
■ D201			$128 \cdot 64^3$	199	4.1	[11(2), 14(2), 16(2), 19(2)]	1078
● N302	3.7	0.0497	$128 \cdot 48^3$	347	4.1	[14, 17, 21, 24]	1383

Table 1: CLS gauge ensembles analysed here. t denotes the source-sink separations and bracketed digits indicate the number of measurements carried out for each distance on each configuration.

For our analysis we employ gauge ensembles generated by the Coordinated Lattice Simulations (CLS) [8] effort, that combine the $N_f = 2+1$ non-perturbatively $\mathcal{O}(a)$ improved Wilson fermionic action with the tree-level Symanzik improved gauge action. To avoid freezing of the topological charge most of these ensembles have open boundary conditions in time [9]. The ensembles are generated along three different trajectories, namely:

- tr$M$ = const: keeping the trace of the quark mass matrix constant near its physical value [8], thereby increasing the strange quark mass while the light quark mass is decreased.
- $\widehat{m}_s \approx \widehat{m}_s^{\text{ph}}$: setting the renormalized strange quark mass to its physical value [10].
- $m_\ell = m_s$: the symmetric line.

This enables us to extrapolate to the physical point along two different quark mass trajectories (tr $M \approx$ tr M^{ph} and $\widehat{m}_s \approx \widehat{m}_s^{\mathrm{ph}}$), while along the symmetric line an extrapolation to the $N_f = 3$ chiral limit can be carried out.

The parameters of the ensembles investigated so far are listed in table 1. These cover a range of pion masses from $\sim 410\,\mathrm{MeV}$ down to $\sim 200\,\mathrm{MeV}$, three different lattice spacings a and volumes with LM_π between 4.1 and 6.4. D201 is on the $\widehat{m}_s \approx \widehat{m}_s^{\mathrm{ph}}$ trajectory, which at this light pion mass is very close to the tr $M = $ const line. H102, N202, N203, N200 and N302 are on the tr $M = $ const line and X250 and X251 (as well as N202) are on the SU(3) symmetric line.

3. Definitions, numerical methods and the fit procedure

The isovector charges are defined as matrix elements of local operators at zero momentum transfer. Here we consider two kinds of (generalized) charges:

$$g_J^B = \langle B | O(\Gamma_J) | B \rangle, \quad J \in \{V, A, T, S\}, \tag{3.1}$$

$$m_B \langle x \rangle_J^B = \langle B | O(\Gamma_J) | B \rangle, \quad J \in \{u^+ - d^+, \Delta u^- - \Delta d^-, \delta u^+ - \delta d^+\}, \tag{3.2}$$

where the Γ-structures of the latter currents contain one derivative and in both cases we use isovector combinations $O(\Gamma_J) = \bar{u}\Gamma_J u - \bar{d}\Gamma_J d$. We destroy the nucleon, the Σ and the Ξ octet baryon components with Dirac index α, using the interpolators

$$N_\alpha = p_\alpha = \varepsilon^{ijk} u_\alpha^i \left(u^{j\mathsf{T}} C \gamma_5 d^k \right), \quad \Sigma_\alpha^+ = \varepsilon^{ijk} u_\alpha^i \left(u^{j\mathsf{T}} C \gamma_5 s^k \right), \quad \Xi_\alpha^0 = \varepsilon^{ijk} s_\alpha^i \left(s^{j\mathsf{T}} C \gamma_5 u^k \right), \tag{3.3}$$

where $q \in \{u, d, s\}$ are Wuppertal smeared quark fields with $m_s \geq m_\ell = m_u = m_d$. When constructing zero-momentum two-point functions $C_{2pt,B}$, we project with $\mathbb{P}_+ = \frac{1}{2}(\mathbb{1} + \gamma_4)$ onto positive parity, while for the three-point functions, we also project on helicity differences if this is required.

The matrix elements are obtained from ratios of three-point over two-point functions

$$R_J^B(t, \tau) = \frac{C_{3pt,B}(t, \tau, \mathbf{q} = \mathbf{p}' = \mathbf{0}, \Gamma_J)}{C_{2pt,B}(t, \mathbf{p} = \mathbf{0})} \xrightarrow{t \gg \tau \to \infty} \langle B | O(\Gamma_J) | B \rangle^{\mathrm{latt}}, \tag{3.4}$$

where t is the temporal source-sink separation and τ the distance of the current from the source. In our case the discretization effects are of orders a^2 and a for matrix elements without and with derivatives, respectively. To quote results in the continuum $\overline{\mathrm{MS}}$ scheme at the scale $\mu = 2\,\mathrm{GeV}$, we renormalize the lattice matrix elements, multiplying these by

$$Z_J(g^2, a\mu) \left(1 + am_\ell b_J(g^2) + 3a\overline{m}\tilde{b}_J(g^2) \right), \tag{3.5}$$

where $3\overline{m} = $ tr M. We non-perturbatively determine the renormalization with respect to the intermediate RI'-SMOM scheme and employ the improvement coefficients $b_J(g^2)$ of [11], where first estimates of $\tilde{b}_J$ were found to be compatible with zero.

With the exception of the $m_\ell = m_s$ ensembles the three-point correlation functions are computed using the stochastic method described in [12] (see also [13, 14, 15, 16]), estimating a timeslice-to-all propagator (depicted as a wiggly line in figure 1). This allows us to factorize the three-point correlation function into two parts, the spectator part S and the insertion part I,

which can be evaluated separately, where we leave all Dirac indices (Greek letters) as well as the stochastic and colour indices (*n* and *k*) open:

$$C(\mathbf{p}',\mathbf{q},x_4',y_4,x_4)_{UDUU}^{\alpha'\alpha\beta'\beta\delta'\delta\gamma'\gamma} = \frac{1}{N_{\text{sto}}} \sum_{n=1}^{N_{\text{sto}}} \sum_{k=1}^{3} \left(S_{UD}(\mathbf{p}',x_4',x_4)_{nk}^{\alpha'\alpha\beta'\beta\delta'} \cdot I_{UU}(\mathbf{q},y_4,x_4)_{nk}^{\delta\gamma'\gamma} \right). \quad (3.6)$$

The baryon source time x_4 and the current insertion time y_4, where the spatial momentum $\mathbf{q}$ is injected, are varied, while the sink time x_4' of the baryon with momentum $\mathbf{p}'$, where the stochastic source is located, is fixed. We have a similar backward sink (not shown) to enable forward-backward time averaging. For the baryons other than the proton, we substitute the quark flavours accordingly. We then compute the contractions for the matrix elements of interest. In this analysis we restrict ourselves to non-flavour changing currents and $\mathbf{p}' = \mathbf{q} = \mathbf{0}$.

Figure 1: The computation of the stochastic three-point function. The red and blue indices correspond to the spectator and insertion part, see eq. (3.6). The blue wiggly line represents the stochastic propagator, whereas solid lines are standard point-to-all propagators.

Note that for different baryon sinks or momenta no additional inversions are needed. However, stochastic noise is added to the gauge noise. This is eventually offset by averaging over three-point functions in the forward and backward directions as well as over equivalent polarizations and momentum combinations at very little computational overhead. Any baryonic three-point function with currents containing (in our case) up to one derivative can be computed at the analysis stage from the building blocks S and I that we store, making this method extremely versatile.

In addition to statistical errors there will be systematic uncertainties related to the precision of the renormalization constants and improvement coefficients, the continuum limit extrapolation, finite volume effects and the use of unphysical quark masses. Not all of these systematics can be explored on the presently analysed subset of CLS ensembles. With all lattice extents $L > 4.1/M_\pi$, finite size effects should be negligible. Before discussing the quark mass dependence, we will study the effect of excited state contributions. For all ensembles we use a set of four different, approximately matched source-sink separations $t/\text{fm} = (x_4' - x_4)/\text{fm} \stackrel{\sim}{\in} \{0.7, 0.8, 1.0, 1.2\}$. In figure 2 we show the ratio R_T^N (see eq. (3.4)) for the tensor channel, in which excited state contributions are clearly visible. To obtain the final result, we carry out simultaneous fits to the two-point function and the ratios using all four (or three) source-sink separations, according to the ansatz

$$C_{2pt,B}(t) = A_0 e^{-m_B t} \left(1 + A_1 e^{-\Delta m_B t}\right), \quad R_J^B(t,\tau) = B_0 + B_1 e^{-\Delta m_B t/2} \cosh(\Delta m_B(\tau - t/2)) + B_2 e^{-\Delta m_B t}$$

$$(3.7)$$

with the mass difference $\Delta m_B = m_B' - m_B$. In these fits the position of the current $\tau = y_4 - x_4$ is allowed to run within the interval $\tau \in [\delta t, t - \delta t]$, where $\delta t \in \{2a, 3a, 4a\}$. Overall, we find stable results for all six fits as can be seen in the bottom right panel of the figure, where the error band indicates our final result.
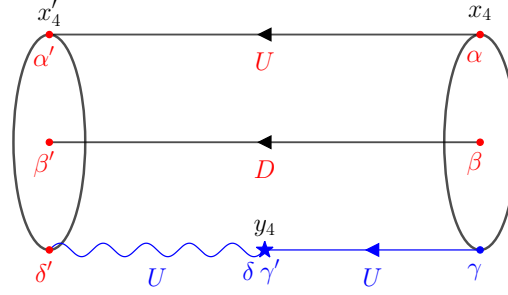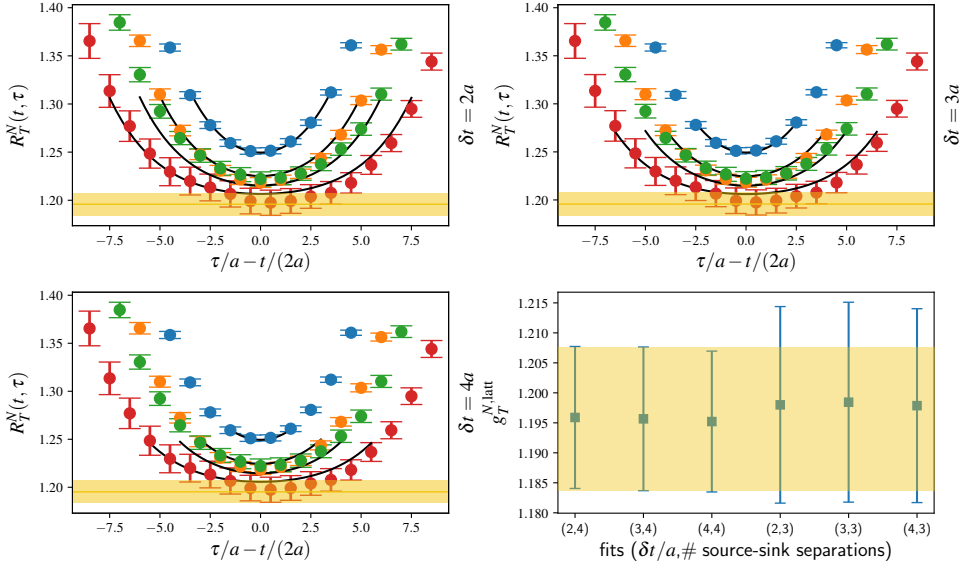
3

Figure 2: Ratios R_T^N (see eq. (3.4)) for the tensor charge of the nucleon g_T^N on ensemble N203 for different source-sink separations t, together with the fits (3.7) covering different intervals $\tau \in [\delta t, t - \delta t]$. We indicate the results of these and three additional fits where we omit the smallest t value in the bottom right panel.
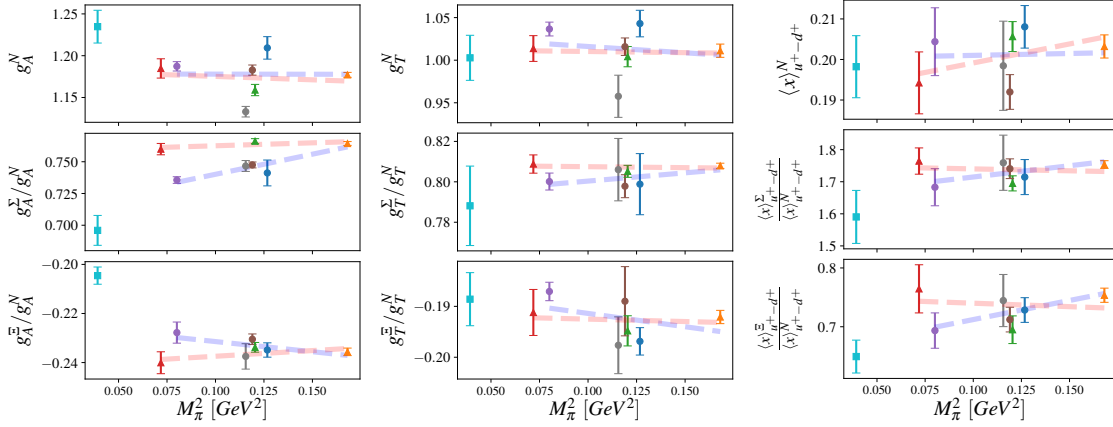
4. Results and Outlook

Figure 3: Axial and tensor charges g_A^B, g_T^B as well as $\langle x \rangle_{u^+ - d^+}^B$, for $B \in \{\Sigma, \Xi\}$ divided by the nucleon's.

In figure 3 we show results for the examples of the axial and tensor charges and the unpolarized isovector PDF Mellin moment $\langle x \rangle_{u^+ - d^+}^B$. The dashed red lines that are drawn to guide the eye connect the $m_\ell = m_s$ points that will approach the SU(3) chiral limit while the blue lines connect the $\text{tr}\, M \approx \text{tr}\, M^{\text{ph}}$ points. The left-most point corresponds to D201, which is on the $\widehat{m}_s \approx \widehat{m}_s^{\text{ph}}$ line, but also near the $\text{tr}\, M = \text{tr}\, M^{\text{ph}}$ trajectory, due to the small pion mass. The first row shows the nucleon charges which are subject to visible cut-off effects. When normalizing hyperon charges with respect to the nucleon charges (second and third rows) the renormalization and improvement factors cancel and the data collapse onto two curves for the two quark mass trajectories, indicating that lattice spacing effects cancel to a large extent.
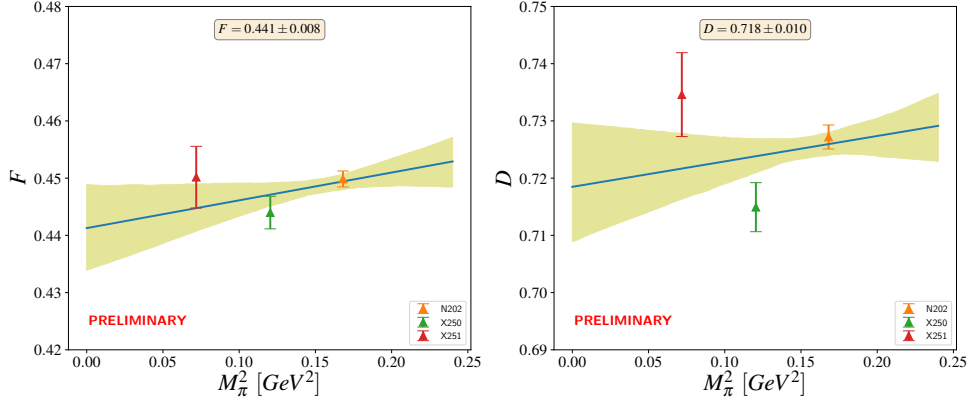
4

Figure 4: Linear extrapolation in M_π^2 of the LECs F and D for the ensembles on the symmetric line.
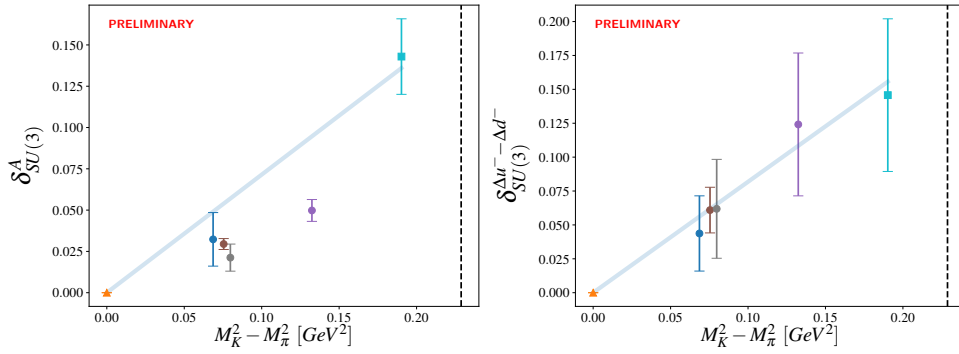

Figure 5: Symmetry breaking parameter (see eq. (4.2)) for g_A and $\langle x \rangle_{\Delta u^- - \Delta d^-}$, where $M_K^2 - M_\pi^2 \propto m_s - m_\ell$. The dashed vertical line indicates the physical point. The blue lines are only drawn to guide the eye.

Assuming SU(3) flavour symmetry, the axial vector charges can be expressed as combinations of the two LECs F and D:

$$g_A^N = F + D, \qquad g_A^\Sigma = 2F, \qquad g_A^\Xi = F - D. \tag{4.1}$$

We can directly extract these LECs, extrapolating the combinations $F = (g_A^N + g_A^\Xi)/2$ and $D = (g_A^N - g_A^\Xi)/2$ along the $m_\ell = m_s$ trajectory as linear functions in M_π^2, see figure 4. Our values are consistent with the recent lattice results obtained in [7], albeit the latter correspond to the SU(2) and not to the SU(3) chiral limit.

Finally, we investigate SU(3) flavour symmetry breaking effects. Note that according to eq. (4.1) $(g_J^N + g_J^\Xi)/g_J^\Sigma = (2F_J)/(2F_J) = 1$ holds for $m_\ell = m_s$. Thus the breaking effect for a current J can, e.g., be quantified in terms of the parameter

$$\delta_{\mathrm{SU}(3)}^J = \left(g_J^N + g_J^\Xi \right)/g_J^\Sigma - 1. \tag{4.2}$$

These effects are small for g_T and $\langle x \rangle_{u^+ - d^+}$ as is also evident from figure 3, where the blue and red data sets do not significantly deviate from each other. However, for the axial moments $g_A = \langle \mathbb{1} \rangle_{\Delta u^+ - \Delta d^+}$ and $\langle x \rangle_{\Delta u^- - \Delta d^-}$ we find symmetry breaking effects of about 10% at physical quark masses, see figure 5. This will be investigated in detail, employing the systematic approach used by QCDSF [5].

We are in the process of analysing additional ensembles that should enable us to carry out controlled physical point and continuum limit extrapolations. We also plan to determine the $\Delta S = 1$ (generalized) form factors to complete the picture of flavour symmetry violation and to determine the relevant baryon ChPT LECs.

References

[1] PARTICLE DATA GROUP: M. Tanabashi et al., *Review of particle physics*, *Phys. Rev. D* **98** (2018) 030001.

[2] H.-W. Lin and K. Orginos, *First calculation of hyperon axial couplings from Lattice QCD*, *Phys. Rev. D* **79** (2009) 034507 [0712.1214].

[3] G. Erkol, M. Oka and T. T. Takahashi, *Axial charges of octet baryons in two-flavor Lattice QCD*, *Phys. Lett. B* **686** (2010) 36 [0911.2447].

[4] QCDSF/UKQCD collaboration: M. Göckeler et al., *Baryon axial charges and momentum fractions with $N_f = 2 + 1$ dynamical fermions*, *PoS* **LATTICE2010** (2010) 163 [1102.3407].

[5] QCDSF/UKQCD collaboration: A. N. Cooke et al., *The effects of flavour symmetry breaking on hadron matrix elements*, *PoS* **LATTICE2012** (2012) 116 [1212.2564].

[6] C. Alexandrou, K. Hadjiyiannakou and C. Kallidonis, *Axial charges of hyperons and charmed baryons using $N_f = 2 + 1 + 1$ twisted mass fermions*, *Phys. Rev. D* **94** (2016) 034502 [1606.01650].

[7] A. Savanur and H.-W. Lin, *Lattice-QCD determination of the hyperon axial couplings in the continuum limit*, 1901.00018.

[8] CLS: M. Bruno et al., *Simulation of QCD with $N_f = 2 + 1$ flavors of non-perturbatively improved Wilson fermions*, *JHEP* **02** (2015) 043 [1411.3982].

[9] M. Lüscher and S. Schaefer, *Lattice QCD without topology barriers*, *JHEP* **07** (2011) 036 [1105.4749].

[10] RQCD collaboration: G. S. Bali, E. E. Scholz, J. Simeth and W. Söldner, *Lattice simulations with $n_f = 2 + 1$ improved wilson fermions at a fixed strange quark mass*, *Phys. Rev. D* **94** (2016) 074501.

[11] P. Korcyl and G. S. Bali, *Non-perturbative determination of improvement coefficients using coordinate space correlators in $N_f = 2 + 1$ lattice QCD*, *PoS* **LATTICE2016** (2016) 190 [1609.09477].

[12] RQCD collaboration: M. Löffler et al., *Baryonic and mesonic 3-point functions with open spin indices*, *EPJ Web Conf.* **175** (2018) 06014 [1711.02384].

[13] R. Evans, G. Bali and S. Collins, *Improved semileptonic form factor calculations in Lattice QCD*, *Phys. Rev. D* **82** (2010) 094501 [1008.3293].

[14] RQCD collaboration: G. S. Bali et al., *Nucleon structure from stochastic estimators*, *PoS* **LATTICE2013** (2014) 271 [1311.1718].

[15] ETM collaboration: C. Alexandrou et al., *A stochastic method for computing hadronic matrix elements*, *Eur. Phys. J. C* **74** (2014) 2692 [1302.2608].

[16] Y.-B. Yang, A. Alexandru, T. Draper, M. Gong and K.-F. Liu, *Stochastic method with low mode substitution for nucleon isovector matrix elements*, *Phys. Rev. D* **93** (2016) 034503 [1509.04616].

[17] Jülich Supercomputing Centre: D. Krause and P. Thörnig, *JURECA: Modular supercomputer at Jülich Supercomputing Centre*, *Journal of large-scale research facilities* **4** (2018) A132.